Sensors and Materials, Vol. 36, No. 12 (2024) 5117–5128
MYU Tokyo

S & M 3856

Wireless Power Transmission by MEMS Vibration Energy Harvester Using Electromagnetic Torque

Akihiro Nomura,* Kensuke Kanda, Takayuki Fujita,
Tsubasa Kuroki, and Kazusuke Maenaka

Graduate School of Engineering, University of Hyogo, 2167, Shosha, Himeji, Hyogo, 671-2280, Japan

(Received July 17, 2024; accepted August 29, 2024)

Keywords: wireless power transmission, MEMS, vibration, energy harvester, electromagnetic torque

We propose a wireless power transfer system using low-frequency magnetic fields. Low-frequency magnetic fields have less effect on the human body and less shielding effect by conductors than high-frequency magnetic fields such as the Qi standard. Therefore, we can explore areas of application in which current high-frequency magnetic field systems cannot be used. The power source is assumed to be a single coil or a Helmholtz coil driven by low-frequency AC current. The power-receiving device has a vibrating beam, which has a Pb(Zr,Ti)O_3 (PZT) layer on the surface, and driving magnets. By applying an AC magnetic field, the beam is vibrated similarly to a tuning fork. The driven force is induced as a torque, and the device can operate even in a parallel magnetic field. The device is realized with MEMS technology and has a volume of 20 × 30 × 0.08 mm^3, a PZT thickness of 10 μm, and a permanent magnet of 9 × 2 × 2 mm^3 attached to it. The device has an output voltage of 3.24 V_{rms} and an output power of 1.54 mW at an applied magnetic flux density of 0.495 mT.

1. Introduction

Energy harvesting technology has attracted attention in IoT and various other fields as a technology for converting small amounts of ambient energy, such as vibrations,[1] light,[2] heat,[3] and radio waves,[4] into electricity. In this paper, a new wireless power transmission system is proposed by combining an AC magnetic source and a vibrating MEMS energy harvester, which is driven by a magnetic field.

In recent years, the practical application of wireless power transmission by magnetic field coupling has been progressing.[5–9] For example, the Qi standard is widely used for electric devices. However, the Qi and many other systems use relatively high frequencies (100–200 kHz).[10] The electromagnetic wave at such a high frequency can affect human health and have a shielding effect by conductors. To broaden the applicability of wireless power transmission, some vibration energy harvesters using bulk magnets have been proposed to realize wireless power transmission at a low frequency.[11–16] Possible uses of the system include supplying power to the inside of a machine surrounded by metal or to medical devices implanted

*Corresponding author: e-mail: ei23u024@guh.u-hyogo.ac.jp
https://doi.org/10.18494/SAM5239

ISSN 0914-4935 © MYU K.K.
https://myukk.org/

in the human body. Thus far, we have developed piezoelectric MEMS energy harvesting devices with 10-μm-thick $Pb(Zr,Ti)O_3$ (PZT) thin films to increase the output power. [17–20] In this study, these piezoelectric harvesting techniques are adopted in the wireless power transmission by electromagnetic coupling using low-frequency (approximately 1000 Hz) AC magnetic fields.

The wireless power transmission assumed in this study is a combination of coil induction and magnet vibration systems. The AC parallel magnetic fields generated by the coil excite the mechanical vibration of the piezoelectric MEMS energy harvester to which magnets are attached. The electro-mechanical coupling of piezoelectric thin films of the harvester outputs electrical energy. In a parallel magnetic field, the magnetic force between the external field and small magnets is canceled out when the magnetic dipole is located along the field. Therefore, the utilization of magnetic torque for the effective magnetic interaction between the parallel magnetic field and the magnets on the harvester is proposed and investigated.

2. Vibration Energy Harvester Using Electromagnetic Torque

2.1 Wireless power transmission using energy harvester

Figure 1 shows a schematic diagram of wireless power transmission. For the transmission system, an AC magnetic field is generated from a coil, through which an electric AC current flows. For the power receiving system, the magnetic field generates force to the permanent magnets on the energy harvester. The magnetic force deforms the beam structure of the harvester. When the beam deforms, the PZT layer on the beam generates electric charges.

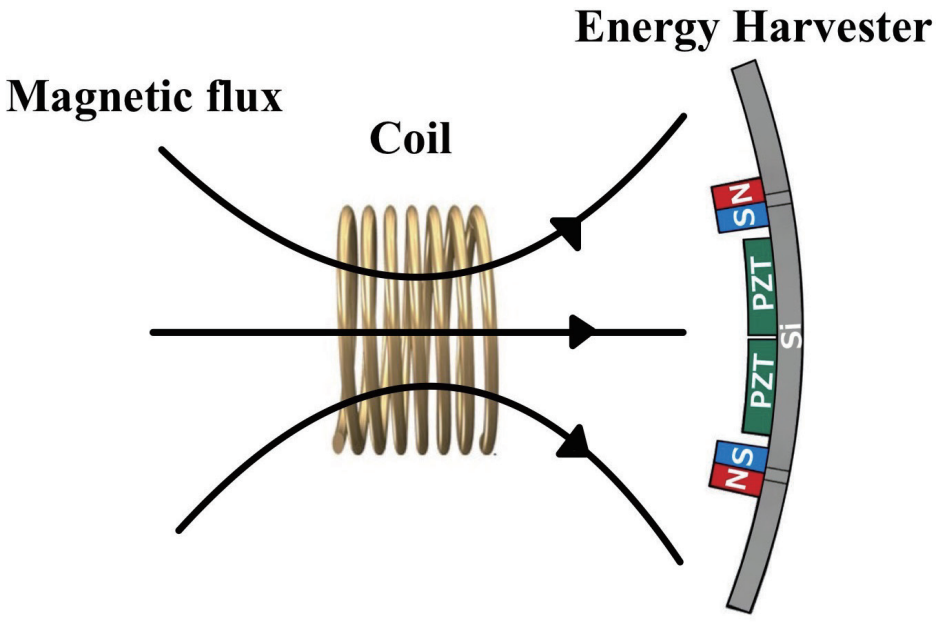

Fig. 1. (Color online) Wireless power transmission using energy harvester.

2.2 Magnetic torque in a magnetic field

Figure 2 shows the forces acting on a magnet in a parallel magnetic field. In a parallel magnetic field, the forces on the magnet are uniform. The magnet in Fig. 2(a) has equal forces at the north and south poles, so the forces cancel each other out. To create a driving force in a parallel magnetic field, the magnet must be driven by torque, as shown in Fig. 2(b). To vibrate a beam with torque, the beam is arranged as shown in Fig. 3(a). Figure 3(b) shows a beam vibrating with torque in a parallel magnetic field.

2.3 Design

The structure in which the beam driven by electromagnetic torque efficiently generates vibration was investigated using the finite element analysis software FEMTET (Murata

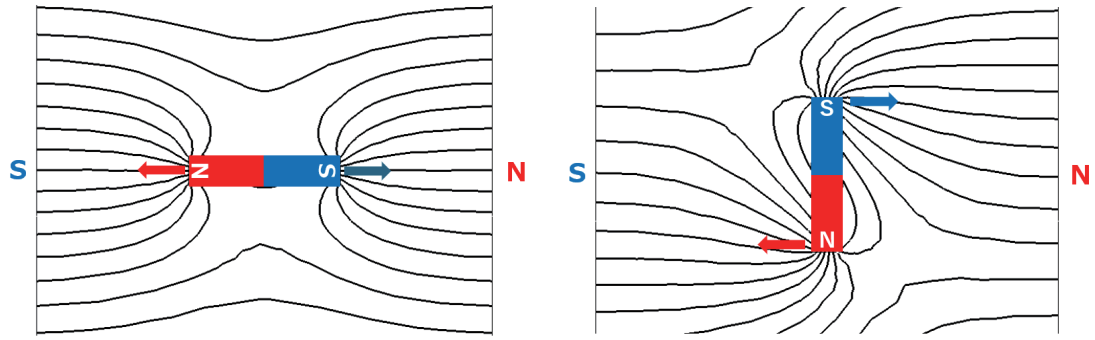

(a) (b)

Fig. 2. (Color online) Forces acting on magnet in parallel magnetic field: (a) linear force. and (b) torque forces.

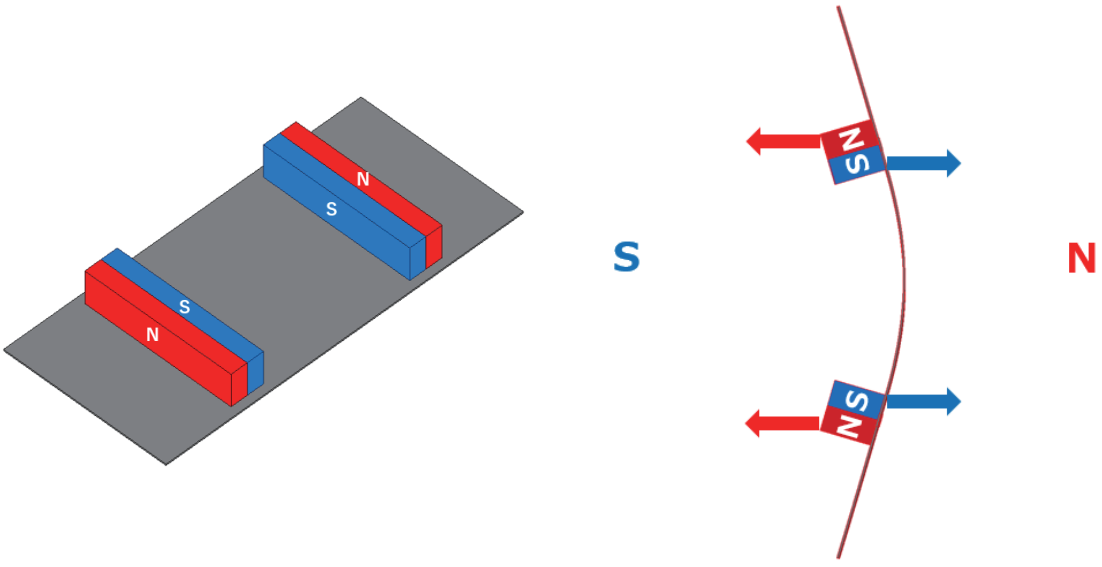

(a) (b)

Fig. 3. (Color online) (a) Magnet placement with torque drive. (b) Vibration modes of beams driven by torque.

Software). First, the displacement profile of the beams at resonance was examined through modal analysis to determine the support point of the beams. The calculation results are shown in Fig. 4. Figures 4(a) and 4(b) show a simple rectangular beam plate and a beam plate with two fixed nodes, respectively. The design is based on the improvement of the Q factor by fixing the non-vibrating nodes. Next, the stress profile was analyzed by modal analysis to determine the location to place the piezoelectric thin film. The calculation results are shown in Fig. 5. The results show that the stress is uniform in the wide center area of the beam. Efficient power transmission is expected by positioning the PZT at the center of the beam where the stress distribution is uniform. The structure of the device on the receiving system is shown in Fig. 6. A silicon-on-insulator (SOI) wafer is used, with the active Si layer (80 μm thick) as the beam structure and the support layer (200 μm thick) as the frame. The piezoelectric effect of the PZT with a large electromechanical coupling coefficient was used for mechanical and electrical energy conversion. The beams deform when an out-of-plane force is applied to the device and the piezoelectric effect of the PZT deposited on the surface of the beams generates an electrical charge on the electrodes. The thicker the PZT film, the higher the output power for the same stress. In this study, the stable deposition of a 10-μm-thick PZT film was achieved by using

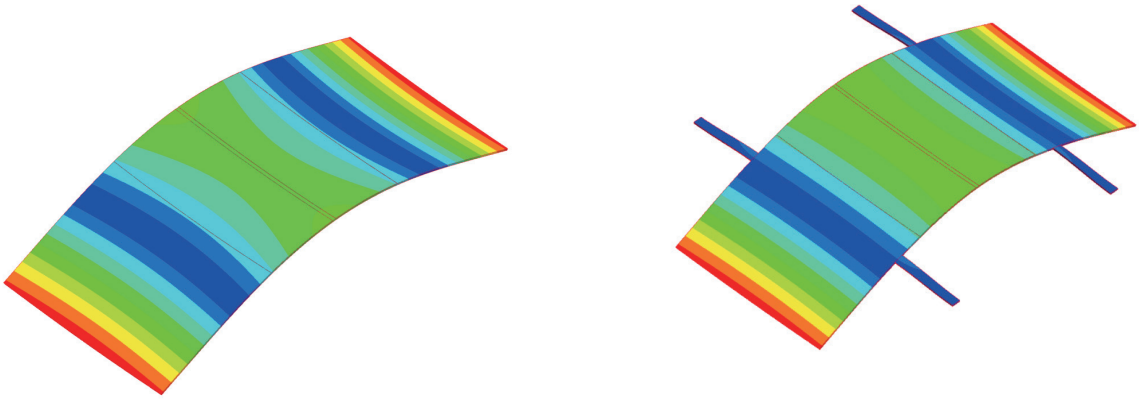

(a) (b)

Fig. 4. (Color online) Displacement distribution from FEM analysis. (a) Rectangular beam plate. (b) Beam plate with two fixed nodes.

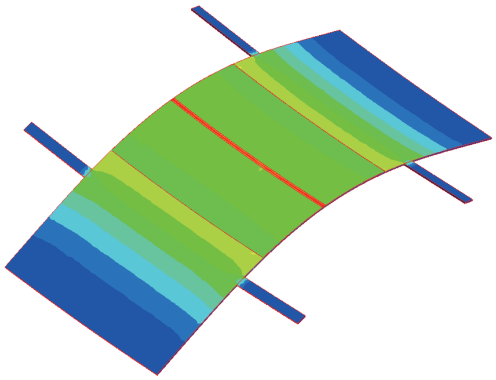

Fig. 5. (Color online) Stress distribution from FEM analysis.

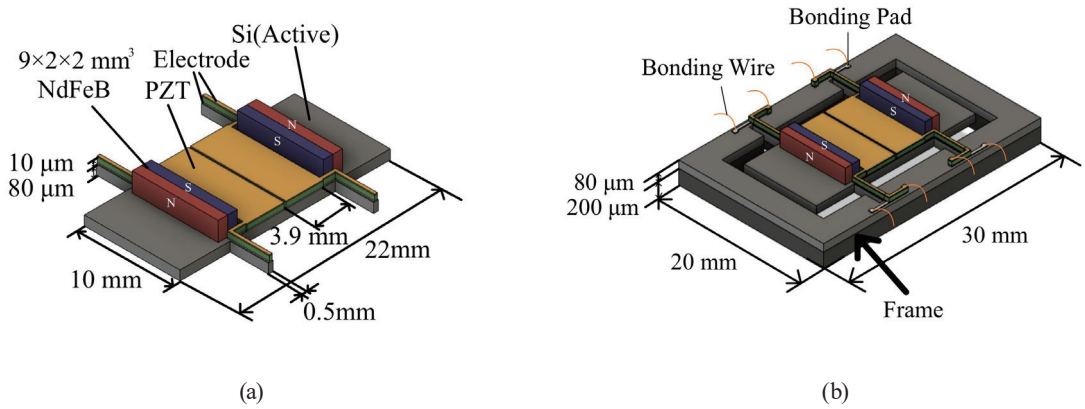

Fig. 6. (Color online) Structure of device. (a) Without frame. (b) With frame.

multilayered sputtering deposition techniques.[21,22] The PZT is divided into two cells, which can be connected in series to increase the output voltage.[23] Magnets were newly fabricated for the appropriate magnetic torque to be achieved as designed. Epoxy resin-based chemically reactive adhesive and neodymium magnetic powder (Magnequench, model number: MQFP-B+) were mixed at a ratio of 1:12. Next, the mixture was poured into a mold shaped by silicone resin and solidified. The mixture was removed from the mold and magnetized by pulsed magnetization at 2.3 kV using a magnetizer (model: M25HS-402). Then, it was formed into a size of 9 × 2 × 2 mm^3, and its surface magnetic flux density was 28.7 mT.

3. Fabrication Process Flow

Figure 7 shows the fabrication process flow. (1) An SOI wafer with an active layer thickness of 80 μm, a support layer thickness of 200 μm, and an insulating layer thickness of 2 μm was used as the starting material. (2) An oxide film was deposited on silicon by thermal oxidation. Next, a 10-μm-thick PZT film was deposited between the Pt/Ti top and bottom electrodes (top electrode thickness: 200 nm; bottom electrode thickness: 100 nm) in a sandwich structure by multilayered deposition techniques.[21,22] (3) The top electrode and PZT were etched simultaneously. The bottom electrode was then etched. Plasma etching using chlorine gas was used for these etching processes that formed PZT cells. Plasma etching has little effect on the PZT thin film. The detailed conditions are the same as previously reported.[17] (4,5) The oxide film was then etched by dry etching, and the active and support layers were etched by deep reactive ion etching to form the device. (6) Finally, the device was attached to a package fabricated by a 3D printer. A photograph of the completed device is shown in Fig. 8.

4. Evaluation

4.1 Measurement environment

A photograph of the actual measurement environment is shown in Fig. 9. A vibration energy harvester is placed on the center axis of the coil. There is a magnetic flux density gradient

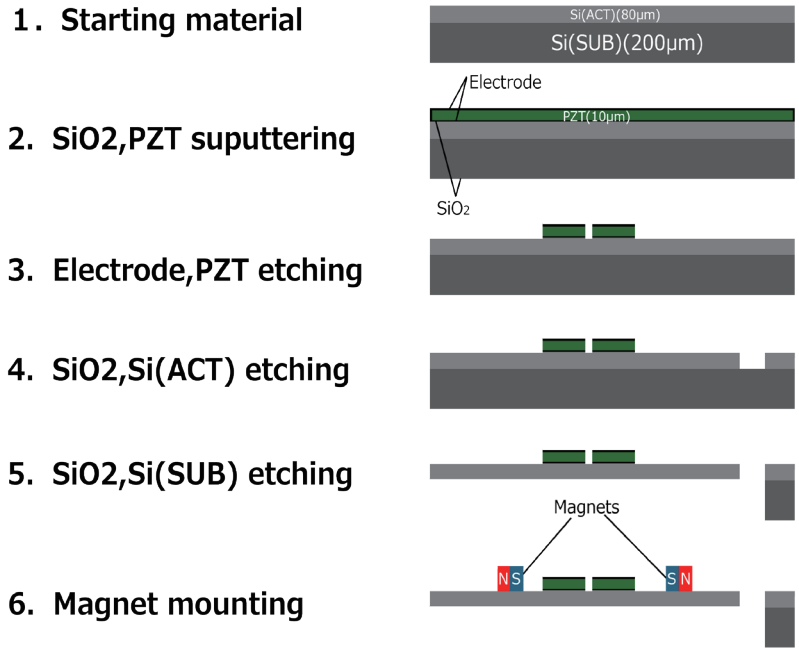

Fig. 7. (Color online) Fabrication process flow.

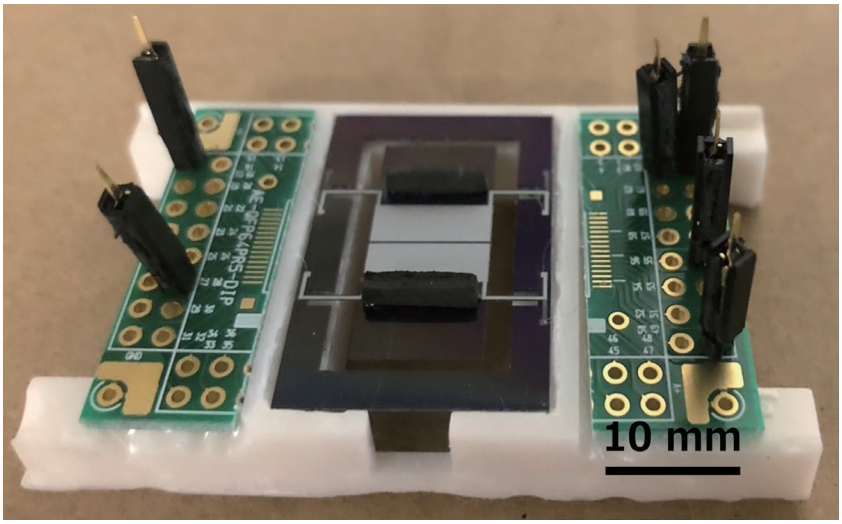

Fig. 8. (Color online) Photograph of fabricated harvester.

around the coil to generate a magnetic field, and a force is generated by the interaction of the coil with the magnetic poles of the permanent magnet. In this case, the size, shape, and placement of the coil are important because the magnetic field distribution is important. However, since this was an initial experiment, a readily available commercial air coil (53 mm diameter, 30 mm width, and 280 turns) was used.

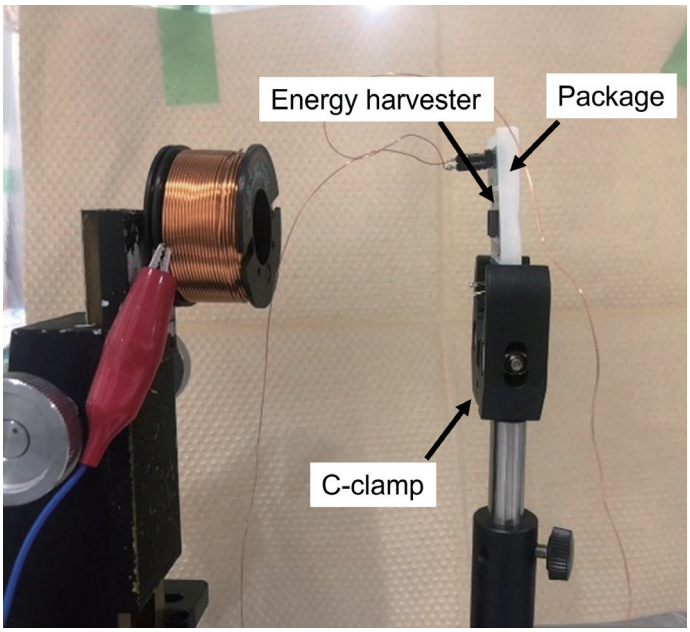

Fig. 9. (Color online) Setup of measurement environment.

4.2 Magnetic flux density against distance

The magnetic flux density was measured against the distance from the surface of the coil. Figure 10 shows the gaussmeter results when a current of 1 A was applied to the coil. The results of the FEM analysis are also shown in the same figure. The measurement results show that the magnetic flux density decreases exponentially with distance. They are also in good agreement with the results of the FEM analysis.

4.3 Output power against distance

The output power was investigated as a function of the distance between the coil and the harvester. In this experiment, the harvester was connected to the optimal load resistance of 3.4 kΩ. This value was derived by calculation based on the PZT capacitance and operating frequency. From the measured values, with a PZT capacitance of C = 45.3 (nF) and an operating frequency of f = 1030 (Hz), the optimal load resistance R_{opt} that maximizes the energy conversion efficiency can be determined as

$$R_{opt} = \frac{1}{2\pi fC}. \tag{1}$$

The output voltage of the device was measured by applying a current of 1 A to the coil, sweeping the frequency, and varying the distance between the coil and the device. The output voltage of one of the PZT cells was measured. The results shown in Fig. 11 are the doubled

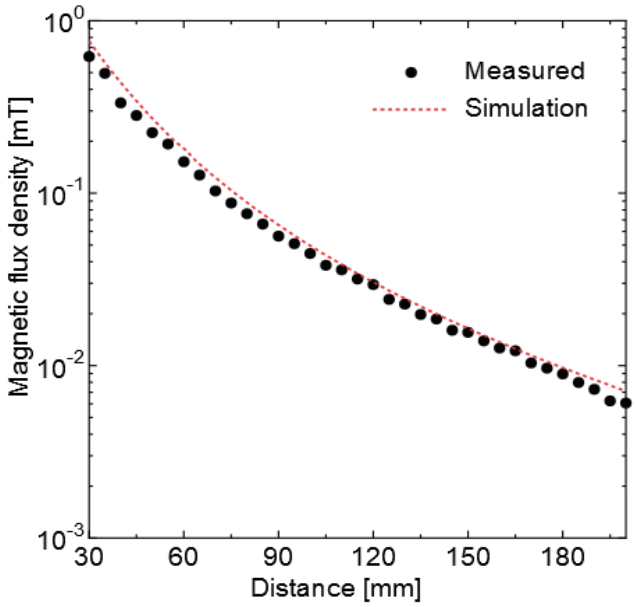

Fig. 10. (Color online) Magnetic flux density against distance.

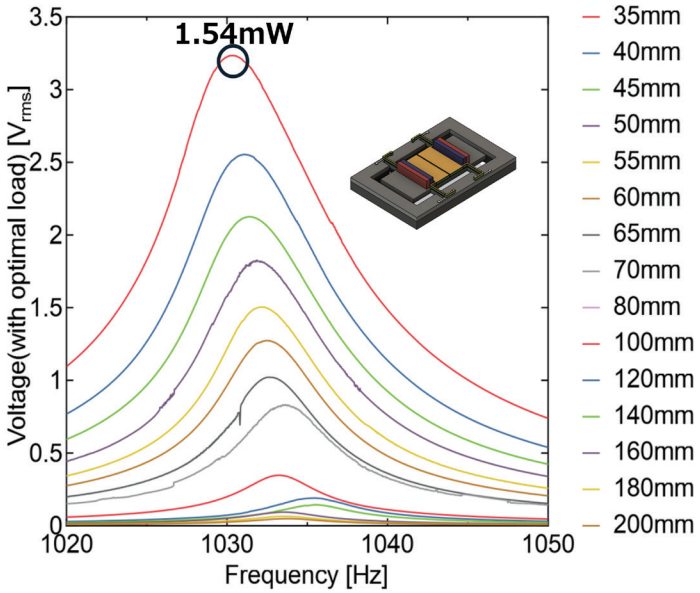

Fig. 11. (Color online) Frequency response of output voltage with optimum load (distance as parameter).

output voltage assuming that two PZT cells are connected in series. Figure 12 shows the graph of the maximum output power from Fig. 11 on the left axis and the magnetic flux density results (Fig. 10) in relation to the distance between the coil and the device on the right axis as a reference. The measurement results show that the output power decreases exponentially with respect to the distance. When the distance was 35 mm, the output voltage was 3.24 V_{rms} and the output power was 1.54 mW. During the examination, acoustic noise is generated by the vibration

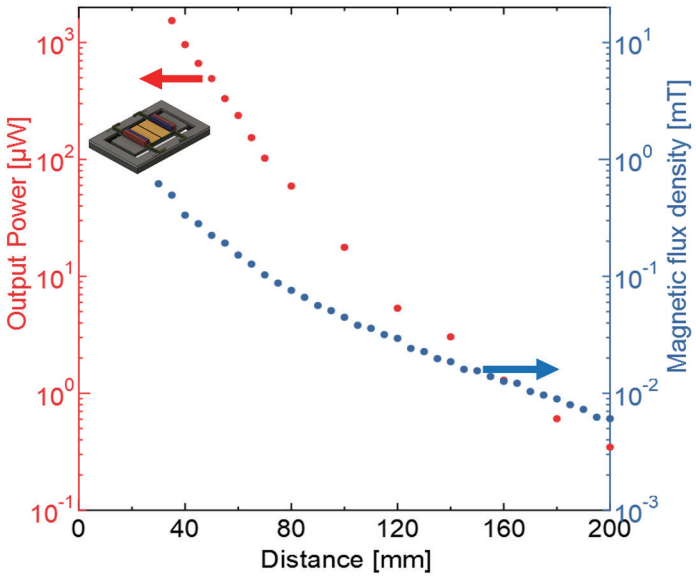

Fig. 12. (Color online) Output power and magnetic flux density versus distance.

of the beam, but it is sufficiently low that it cannot be heard if the listener's ear is more than a few centimeters away from the device.

5. Results and Discussion

We discuss whether the output power from this study is sufficient to power other devices. Assuming the system that the harvested power is used for radio communication by a Bluetooth low-energy (BLE) beacon. BLE beacons typically require approximately 100 μJ of power to operate.[24–26] The energy harvester in this study can transmit BLE beacon signals approximately 15 times per second, confirming sufficient power supply for sensing. We also compared the output power of the energy harvester in this study with those in other studies. The low-frequency wireless power transmissions using various other piezoelectric energy harvesters were compared.[11–16] Table 1 shows the resonant frequency [Hz], magnetic flux density received from the coil (mT), size (mm^3), power generation (μW), and normalization value [$\mu W/(mm^3 \times mT^2)$] for the devices in the other studies. The table confirms that the normalized performance of the device in this study is approximately 4–30 times higher than those of the other devices. The superior performance is attributed to the miniaturization achieved by MEMS technology.

6. Conclusions

In this study, we proposed wireless power transmission by a MEMS vibration energy harvester using electromagnetic torque that can be used even in a parallel magnetic field. When the distance between the coil and the device was 35 mm (magnetic flux density from the coil: 0.495 mT), an output voltage of 3.24 V_{rms} and an output power of 1.54 mW were obtained. The

Table 1
Low-frequency wireless power transmissions using various energy harvesters.

	Frequency (Hz)	Magnetic flux density received from coil (mT)	Size (mm^3)	Output power (μW)	Normalization value [$\mu W/(mm^3 \times mT^2)$]
This study	1030	0.495	240	1540	26.2
Ref. 11	98.9	0.1	1245	14.6	1.17
Ref. 12	64	0.1003	Not specified	3.4	Not specified
Ref. 13	350	0.1197	103	1.3	0.88
Ref. 14	108.5	0.0895	68	0.9	1.65
Ref. 15	211	0.85	743	3300	6.15
Ref. 16	724	1.8	85.7	360	1.3

device in this study was able to transmit BLE beacon signals approximately 15 times per second, confirming sufficient power supply for sensing. The devices in this study showed an approximately 4–30 times higher normalized performance than those in other studies.

Acknowledgments

This work was supported in part by the Japan Society for the Promotion of Science (JSPS) Grant Numbers 20H02120 and 22K04897.

References

1 A. Shirane, H. Ito, N. Ishihara, and K. Masu: Jpn. J. Appl. Phys. **54** (2015) 04DE11. https://doi.org/10.7567/JJAP.54.04DE11
2 Z. Yi, B. Yang, G. Li, J. Liu, X. Chen, X. Wang, and C. Yang: Appl. Phys. Lett. **111** (2017) 013902. https://doi.org/10.1063/1.4991368
3 L. L. Kazmerski: Renewable Sustainable Energy Rev. **1** (1997) 71. https://doi.org/10.1016/S1364-0321(97)00002-6
4 E. Shoji: Energy Technol. **12** (2023) 2300604. http://doi.org/10.1002/ente.202300604
5 S. Y. R. Hui, W. Zhong, and C. K. Lee: IEEE Trans. Power Electron. **29** (2014) 4500. https://doi.org/10.1109/TPEL.2013.2249670
6 A. P. Sample, D. A. Meyer, and J. R. Smith: IEEE Trans. Ind. Electron. **58** (2011) 544. https://doi.org/10.1109/TIE.2010.2046002
7 S. Cheon, Y. H. Kim, S. Y. Kang, M. L. Lee, J. M. Lee, and T. Zyung: IEEE Trans. Ind. Electron. **58** (2011) 2906. https://doi.org/10.1109/TIE.2010.2072893
8 Z. H. Ye, Y. Sun, X. Dai, C. S. Tang, Z. H. Wang, and Y.-G. Su: IEEE Trans. Power Electron. **31** (2016) 4809. https://doi.org/10.1109/TPEL.2015.2483839
9 Y. Zhang, Z. Zhao, and K. Chen: IEEE Trans. Ind. Appl. **50** (2014) 2436. https://doi.org/10.1109/TIA.2013.2295007
10 W.-F. Brou, Q.-T. Duong, and M. Okada: IEICE Trans. Electron. **E106.C** (2023) 165. https://doi.org/10.1587/transele.2022ECP5013
11 G. Liu, P. Ci, and S. Dong: Appl. Phys. Lett. **104** (2014) 032908. https://doi.org/10.1063/1.4862876
12 B. D. Truong, D. Wang, T. Xue, S. Trolier-Mckinstry, and S. Roundy: J. Phys. Conf. Ser. **1407** (2019) 012063. https://doi.org/10.1088/1742-6596/1407/1/012063
13 B. D. Truong, and S. Roundy: Smart Mater. Struct. **28** (2019) 015004. https://doi.org/10.1088/1361-665X/aaeb6a
14 B. D. Truong, S. Williams, and S. Roundy: J. Intell. Mater. Syst. Struct. **30** (2019) 2464. https://doi.org/10.1177/1045389X19862383

15 M. A. Halim, J. M. Samman, S. E. Smith, and D. P. Arnold: 2019 19th Int. Conf. Micro and Nanotechnology for Power Generation and Energy Conversion Applications (PowerMEMS, 2019) 1–5. https://doi.org/10.1109/PowerMEMS49317.2019.20515809768
16 M. A. Halim, A.A. Rendon-Hernandez, and D. P. Arnold: 2020 IEEE PELS Workshop Emerging Technologies: Wireless Power Transfer (WoW, 2020) 271–274. https://doi.org/10.1109/WoW47795.2020.9291290
17 K. Kanda, S. Hirai, T. Fujita, and K. Maenaka: Sens. Actuators, A **281** (2018) 229. https://doi.org/10.1016/j.sna.2018.09.018
18 S. Hirai, K. Kanda, T. Fujita, and K. Maenaka: Jpn. J. Appl. Phys. **58** (2019) SLLD07. https://doi.org/10.7567/1347-4065/ab362f
19 K. Kanda, T. Aiba, and K. Maenaka: Sens. Mater. **34** (2022) 1879. https://doi.org/10.18494/SAM3867
20 T. Yokota, K. Kanda, T. Fujita, and K. Maenaka: IEEJ Tras. SM. **143** (2023) 256. https://doi.org/10.1541/ieejsmas.143.256. (in Japanese)
21 K. Kanda, T. Koyama, T. Yoshimura, S. Murakami, and K. Maenaka: IEEE Trans. Ultrason. Ferroelectr. Freq, **68** (2021) 1988. https://doi.org/10.1109/TUFFC.2020.3039230
22 R. Sano, J. Inose, K. Kanda, T. Fujita, and K. Maenaka: Jpn. J. Appl. Phys. **54** (2015) 10ND03. https://doi.org/10.7567/JJAP.54.10ND03
23 K. Kanda, T. Saito, Y. Iga, K. Higuchi, and K. Maenaka: Sensors **12** (2012) 16673. https://doi.org/10.3390/s121216673
24 E. MacKensen, M. Lai, and T. M. Wendt: Proc. IEEE Sens. (2012). https://doi.org/10.1109/ICSENS.2012.6411303
25 M. Siekkinen, M. Hiienkari, J. K. Nurminen, and J. Nieminen: 2012 IEEE Wireless Communications and Networking Conf. Workshops (WCNCW, 2012) 232–237. https://doi.org/10.1109/WCNCW.2012.6215496
26 X. Fafoutis, B. Janko, E. Mellios, G. Hilton, R. S. Sherratt, R. Piechocki, and I. Craddock: Lect. Notes Comput. Sci. (2017) 294. https://doi.org/10.1007/978-3-319-49655-9_37

About the Authors

Akihiro Nomura received his B.E. in electrical engineering from the University of Hyogo, Japan, in 2023. Since 2023, he has been a Master's student at the University of Hyogo. Currently, he is researching MEMS vibration energy harvesters. (ei23u024@guh.u-hyogo.ac.jp)

Kensuke Kanda received his B. E., M. E., and Ph. D. degrees in mechanical engineering from Tokyo Metropolitan University, Japan, in 2000, 2003, and 2006, respectively. From 2006 to 2008, he worked as a postdoctoral researcher in the Advanced Software Technology and Mechatronics Research Institute of Kyoto, Japan. From 2008 to 2010, he worked for the Maenaka Human-Sensing Fusion Project at Japan Science and Technology Agency, Japan. Since 2010, he has been with the University of Hyogo, where he is currently an associate professor. His research interests include piezoelectric microdevices and systems. (kanda@eng.u-hyogo.ac.jp)

Takayuki Fujita received his B. E., M. E., and Ph. D. degrees from the Himeji Institute of Technology, Japan, in 1995, 1997, and 2000, respectively. Since 2001, he has been a research associate at the Himeji Institute of Technology. He is currently a professor at the Advanced Medical Engineering Research Institute, University of Hyogo. His research interests include MEMS, energy harvesting, and IoT devices for healthcare. (fujita@ame.u-hyogo.ac.jp)

Tsubasa Kuroki received his B.E. in electrical engineering from the University of Hyogo, Japan, in 2023. Since 2023, he has been a Master's student at the University of Hyogo. Currently, he is researching artificial intelligence for counseling. (k.skywing@gmail.com)

Kazusuke Maenaka received his B. E., M. E., and Ph. D. degrees from Toyohashi University of Technology, Japan, in 1982, 1984, and 1990, respectively. Since 1993, he has been with the Department of Electronics at the Himeji Institute of Technology. With the unification of universities in the Hyogo prefecture in April 2004, he joined the University of Hyogo, where he is presently a professor. Since 2008, he has been the project leader of the Maenaka Human-Sensing Fusion Project supported by the Japan Science and Technology Agency. His research interests include MEMS devices and technology, especially silicon mechanical sensors and their integration. (maenaka@eng.u-hyogo.ac.jp)